European Journal of Human Genetics (2009) 17, 14–21

www.nature.com/ejhg

ARTICLE

Syndromic congenital sensorineural deafness, microtia and microdontia resulting from a novel homoallelic mutation in fibroblast growth factor 3 (*FGF3*)

Osama Alsmadi[1], Brian F Meyer[1], Fowzan Alkuraya[1], Salma Wakil[1], Fadi Alkayal[1], Haya Al-Saud[1], Khushnooda Ramzan[1] and MoeenAldeen Al-Sayed*[,2]

[1]*Arabian Diagnostic Laboratories, Department of Genetics, Research Center, King Faisal Specialist Hospital & Research Center, Riyadh, Saudi Arabia;* [2]*Department of Medical Genetics, King Faisal Specialist Hospital & Research Center, Riyadh, Saudi Arabia*

We identified a homozygous missense mutation (c.196G→T) in fibroblast growth factor 3 (*FGF3*) in 21 affected individuals from a large extended consanguineous Saudi family, phenotypically characterized by autosomal recessive syndromic congenital sensorineural deafness, microtia and microdontia. All affected family members are descendents of a common ancestor who had lived six generations ago in a geographically isolated small village. This is the second report of *FGF3* involvement in syndromic deafness in humans, and independently confirms the gene's positive role in inner ear development. The c.196G→T mutation results in substitution of glycine by cysteine at amino acid 66 (p.G66C). This residue is conserved in several species and across 18 FGF family members. Conserved glycine/proline residues are central to the 'β-trefoil fold' characteristic of the secondary structure of FGF family proteins and substitution of these residues is likely to disrupt structure and consequently function.
European Journal of Human Genetics (2009) **17,** 14–21; doi:10.1038/ejhg.2008.141; published online 13 August 2008

Keywords: syndromic deafness; sensorineural; Arab; consanguineous; FGF; congenital

Introduction

Approximately one in 1000 children is affected by severe or profound hearing loss at birth or during childhood (pre-lingual deafness). About 60% of these cases are hereditary, 30% acquired, and 10% are idiopathic.[1] Impaired auditory function can be the only clinical manifestation (non-syndromic deafness; 70%) or be associated with other symptoms or anomalies (syndromic deafness; 30%). Both forms may result from classical Mendelian inheritance. Based on anatomical defects hearing loss may also be classified as conductive or sensorineural. Conductive hearing loss is associated with external ear or middle ear abnormalities, whereas sensorineural deafness is caused by defects anywhere from the cochlea (inner ear) to the auditory cerebral cortex.[2]

The inner ear is a morphologically complex sensory organ responsible for hearing and balance, and its dysfunction is among the most common congenital disorders.[3,4] In the murine system, morphogenesis and differentiation of the otic epithelium involves signaling interactions within and between otic and non-otic tissues. Fibroblast growth factor (FGF) signals are required for expression of otic placode genes and for otic placode induction and vesicle

*Correspondence: Dr MA Al-Sayed, Department of Medical Genetics, King Faisal Specialist Hospital & Research Center, P.O. Box 3354, MBC 75, Riyadh 11211, Saudi Arabia.
Tel: +96 612 055 162; Fax: +96 612 055 171;
E-mail: moeen@kfshrc.edu.sa
Received 5 January 2008; revised 26 June 2008; accepted 2 July 2008; published online 13 August 2008

formation. These signals are likely to be provided, in mice, by *fgf8*, *fgf10,* and *fgf3*, expressed by the endoderm, mesenchyme and hindbrain, respectively.[5–7] Wnt signals are also required for otic placode formation.[8] FGF signaling and its role in otic vesicle formation was also demonstrated in a chick embryo model. FGF signaling inhibition by SU5402 was shown to result in a dose-dependent alteration of otic canal formation.[9] Mice mutants lacking *fgfr2b* form otic vesicles which subsequently develop dysmorphologies at the endolymphatic duct and sac, including outgrowth plus failure of semicircular canal formation.[10] Most *fgf10* mutants completely lack semicircular canals.[11,12] *fgf3*-null mutants undergo normal otic vesicle formation, but then go on to develop highly variable and incompletely penetrant inner ear dysmorphologies that like those of *fgfr2b* mutants, appear to initiate at the endolymphatic duct and sac outgrowth stage. Very recently *fgf3* was shown to be required for dorsal otic patterning and the gene's primary role was to maintain and focus the dorsal otic gene expression induced by Wnt signals, and highlighting a new example of cross talk between the two signaling systems.[13]

Aside from a recent report,[13] the involvement of FGFs and their role in the evolutionary and developmental origin of the human inner ear are largely unknown. In this paper, we report on an extended Arab family, from a geographically isolated village in Saudi Arabia, with recessively inherited profound bilateral congenital deafness, bilateral microtia, inner ear agenesis, as well as small incisor and canine teeth. We describe use of a positional candidate approach and identification of novel missense mutation in *FGF3* and the associated phenotype.

Materials and methods

Human subjects

Approval for this study was obtained from the Institutional Review Board (IRB) of King Faisal Specialist Hospital and Research Centre, Riyadh, Saudi Arabia. We ascertained and recruited a highly consanguineous family from an isolated village in Saudi Arabia, with a total population of approximately 600. A pedigree was constructed for this large multi-generational family with an apparently syndromic recessive pattern of hearing loss (Figure 1). Forty individuals from this family were recruited including 21 deaf subjects. The individuals are descendents of a common ancestor who had lived six generations ago in that village. Signed informed consent was obtained from

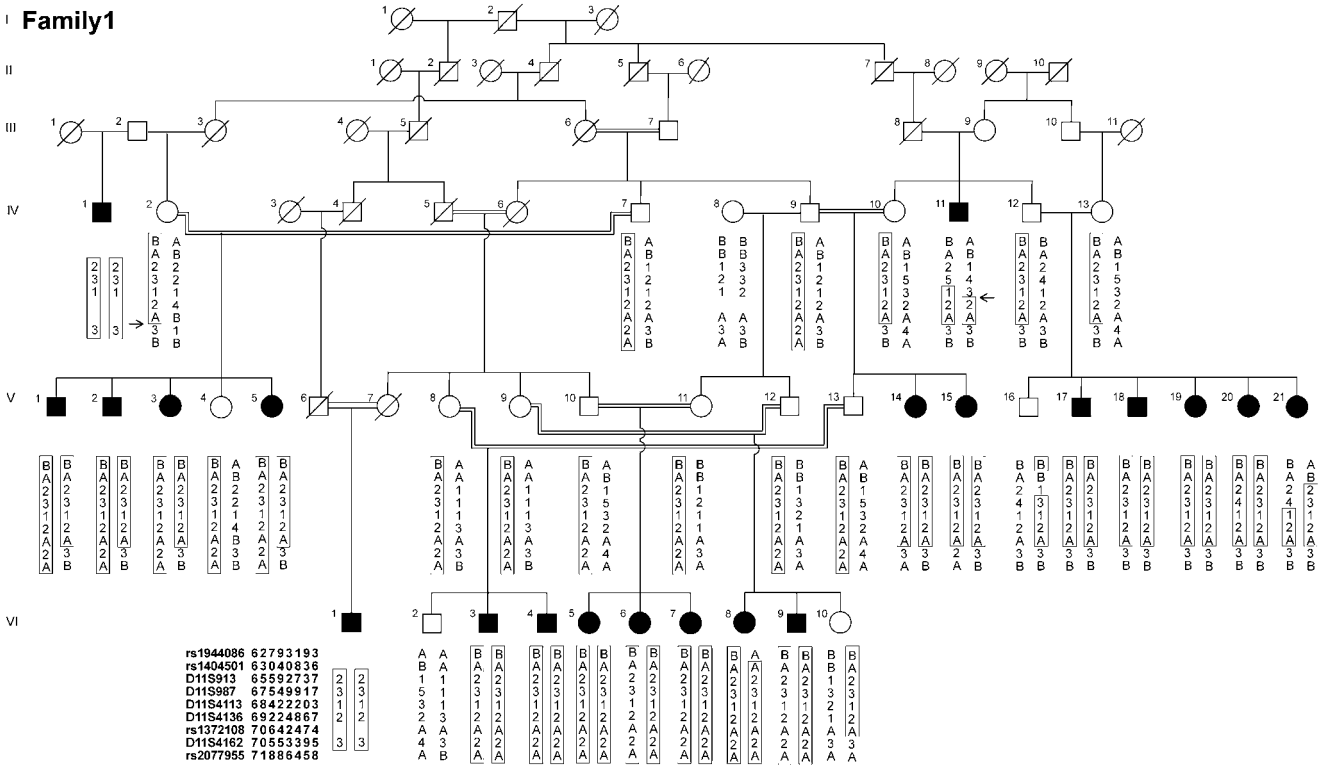

Figure 1 Families' pedigree of family members whose DNA was studied or who are necessary to construct the pedigrees are represented. Affected family members are represented by solid symbols, male family members by squares, and female members by circles. The most likely haplotype for chromosome 11 SNPs and microsatellite markers is shown. The boxed portion of the bars indicates the haplotypes linked to the gene for deafness in each branch of the pedigree.

all participants. A parent or legal guardian supplied a written consent for children who were under the age of 18. Complete physical, clinical, and ophthalmologic examinations, pure-tone audiometry, tympanometry, otoacoustic emission test, computed tomography (CT) and magnetic resonance imaging (MRI) were conducted in the index case. The remaining volunteer phenotypes were examined thoroughly onsite in their resident village during sample collection.

DNA isolation

Peripheral blood samples were obtained through venipuncture. In some instances, dried blood spots were collected by thumb or heel prick due to age limitations and/or volunteers' preference. Genomic DNA was extracted by standard techniques[14] from whole blood samples, and in the case of dried blood spots multiple displacement amplification was utilized to obtain sufficient DNA for analysis.[15]

Whole genome scan

A genomewide scan of selected family members was undertaken using the GeneChip Mapping 10K 2.0 *Xba*I array which contained 11 560 SNPs with an average distance of 0.31 cM. SNP genotyping was performed using the Affymetrix protocol for 10K *Xba*I arrays with minor modifications.[16] In brief, 250 ng of genomic DNA isolated from peripheral blood was digested per sample, with the restriction endonuclease *Xba*I, for 2.5 h at 37°C. Digested DNA was mixed with *Xba*I adapters and ligated, using T4 DNA ligase, for 2.5 h at 37°C. Ligated DNA was added to four separate PCRs of 100 μl each, cycled, pooled, and then purified to remove unincorporated dNTPs. The purified PCR products were then fragmented and labeled with biotin-dATP. Biotin-labeled DNA fragments were hybridized to the 10K *Xba*I array for 18 h, washed stained and scanned as recommended by the manufacturer. Using raw data, allele calling was then performed using GeneChip DNA Analysis Software (GDAS) v.3.0. Genotype data was checked for Mendelian inconsistencies using the shareware application PedCheck.[17] Genotypes showing discrepancies were discarded at that marker for all members of the pedigree being analyzed. Non-Mendelian errors detected through unlikely recombinants were identified and removed using the Merlin software package.[18] Multi point parametric linkage analysis was performed using the Allegro (version 1.2) module of easyLINKAGE plus v5.02.[19] A recessive model of inheritance was assumed with a population disease allele frequency of 0.0001 and equal SNP allele frequencies.

Fine mapping

Five microsatellite markers (D11S913, D11S987, D11S4113, D11S4136, and D11S4162), within the linkage interval identified using SNP analysis, were used to increase information content and to narrow critical region prior to selecting positional candidate genes for sequencing. PCR amplification was performed on a thermocycler (DNA Engine Tetrad MJ Research, USA) in a total volume of 25 μl, containing 10 ng DNA, 50 mM KCl, 10 mM Tris-HCl (pH 9.0), 1.5 mM $MgCl_2$, 0.1% Triton X-100, 0.25 mM of each dNTP, 0.8 pM of each primer (one fluorescently labeled) and 0.5 U of Taq polymerase (QIAGEN, D-40724, Hilden, Germany). For PCR, an initial denaturation step at 95°C for 10 min was followed by 40 cycles of denaturation at 95°C for 30 s, annealing at 58°C for 30 s and extension at 72°C for 30 s followed by a final extension step of 72°C for 10 min. PCR products were separated using a MegaBace 1000 capillary sequencer and sized using the Genetic Profiler software package (Amersham, Sunnyvale, CA, USA). Pedigrees were drawn and inferred haplotypes were represented based on parental genotypes using Cyrillic Version 2.1.3 software (Cherwell Scientific, Oxford, UK).

Sequencing of positional candidate genes

Candidate genes from within the critical region identified following fine mapping were screened for mutation using direct sequencing. Primers were designed and optimized for the entire coding region of all candidate genes. The primer sequences are available from the authors upon request. PCR amplifications were performed in 25 μl reactions in essence as previously described.[20] PCR products were sequenced using the DYEnamic ET Dye Terminator Cycle Sequencing Kit (Amersham Biosciences; Piscataway, NJ, USA; www.amersham.com) on a MegaBACE 1000 DNA Analysis System (Molecular Dynamics; Sunnyvale, CA, USA). Sequence data was aligned to reference GenBank sequences and examined for variation.

Results

Patients and clinical presentation

At the time of enrollment, the proband (patient VI:8) a 4-year-old girl was diagnosed with profound bilateral congenital deafness, bilateral microtia and microdontia. Her pregnancy was uneventful without any history of antenatal exposure to drugs, radiation or infection. Delivery was vaginal with a birth weight of 3 kg. She had repeated chest infections starting at the age of 21 months requiring hospitalization, which was resolved by the age of 3 years. Physical examination revealed normal weight at 50th, height at 5th, and head circumference at 10th centiles. Intelligence, motor and psychosocial developments were normal. Facial features were normal apart from a prominent tip of the nose (Figure 2a), dysplastic ears, bilateral type 1 microtia (Figure 2b and c), and microdontia with widely spaced teeth (Figure 2d). The ears were also low set and anterverted. Dysplastic ear changes were asymmetrical and more pronounced in the upper half. Both

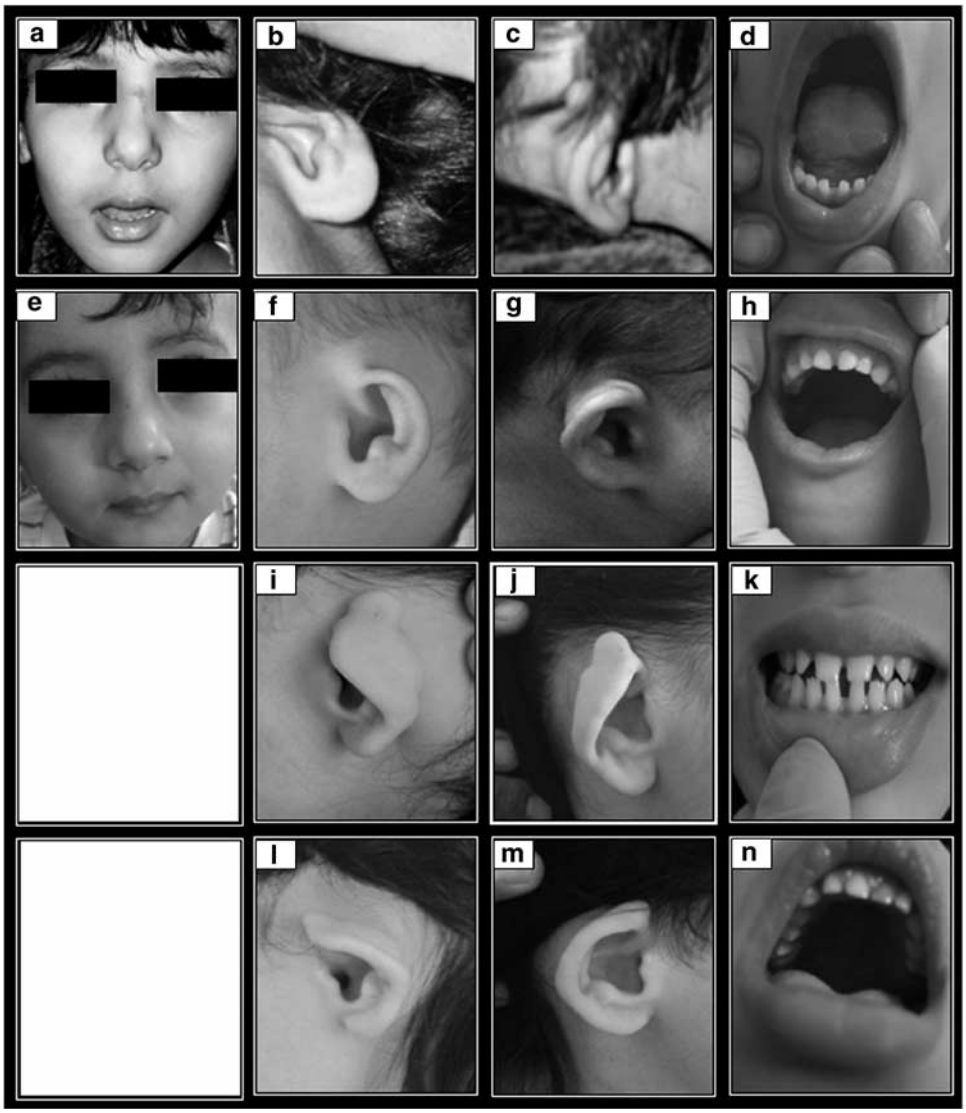

Figure 2 Clinical photographs of some of the affected individuals. The index case, VI:8 from Figure 1, showing (**a**) the prominent tip of the nose, (**b** and **c**) low set, anterverted, dysplastic left and right ears, and (**d**) small widely spaced teeth. Dysplastic ear changes were asymmetrical and more pronounced in the upper half. The right ear was more severely affected and also the upper part of right helix was more lobulated. Affected individual VI:9 shares the same facial features including (**e**) tip of nose, (**f** and **g**) ears, and (**h**) teeth. Patients VI:6 (**i**–**k**) and VI:7 (**l**–**n**) also share similar facial malformations. The affected individuals in this family present some intrafamilial variability in the severity of these malformations.

external auditory meatuses were patent with no stenosis. The right ear was more severely affected and also the upper part of right helix was more lobulated (Figure 2c). Incisors and canine teeth were small and misaligned with increased space between the teeth. Incisors were also thinner than average, with abnormal notching of the upper part (lower incisors) (Figure 2d). No palatal abnormalities or other skeletal deformities were detected. Ophthalmoscopic evaluation showed normal retinal findings. Cardiovascular, abdominal, central nervous system and rest of physical examinations were normal. TORCH screen for cytomegalovirus, herpes simplex virus, rubella and toxoplasma was negative. Complete blood count, serum electrolytes and results of liver and renal functions were all within normal limits.

Type A and type B tympanograms were recorded in right and left ear respectively. Otoacoustic emission were absent across the entire frequency range from both ears indicating outer hair cell dysfunction. Brain stem auditory evoked potentials were absent bilaterally indicating a profound hearing loss.

CT of the temporal bones (Figure 3) revealed asymmetric tympanic cavities on both sides. The outer auditory canals, eardrums and middle ear ossicles were present and normal,

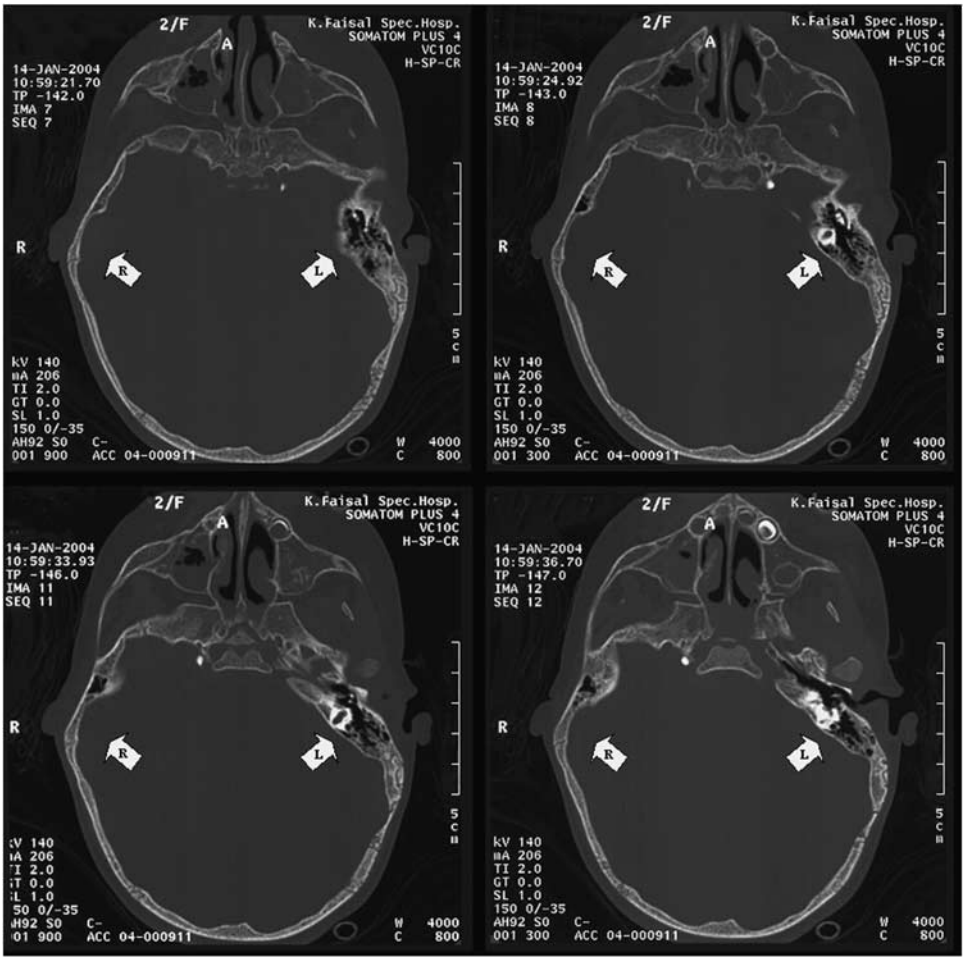

Figure 3 CT scans of the temporal bones. All four panels are showing asymmetric tympanic cavities. On the right side vestibular or cochlear system was not visualized; however, a cystic vestibulum was recognized on the left side.

while the inner auditory canals were not visible. On the right side vestibular or cochlear system was not visualized, however, a cystic vestibulum was recognized on the left side. Magnetic resonance imaging MRI of the ear structures revealed an unidentifiable right ear internal auditory canal and a poorly visualized left one. Inner ear structure revealed absent cochlea bilaterally with rudimentary vestibular structures and no semicircular canals. On the left side, one nerve was present within the internal auditory canal, which may actually be the facial nerve and on the right side no neural structure that may correspond to components of the cochlear vestibular bundle was identified. Brain MRI revealed a normal corpus callosum. Axial T2-weighted images revealed a persistently hyperintense cerebral white matter in the temporopolar areas and in the subinsular regions indicating delayed mylenation. The most recent follow up was at the age of 6 years and 5 months. Her physical development remained normal (weight at 50th, height at 45% and head circumference at 25% centiles).

Her affected brother (individual VI:9 in Figure 1) with profound bilateral congenital deafness, microtia, and microdontia was seen at the age of 3 years. He has normal growth (weight, height, and head circumference were at 40th, 25th, and 40th centiles respectively), and normal cognitive development. Regarding facial features, the tip of the nose was prominent (Figure 2e) with widely spaced small teeth (Figure 2h). His ears were also low set and anteverted. The upper part of the right ear was more severely affected with anteversion and lobulation of helix at the upper end (Figure 2f and g). The rest of the physical examination was normal.

The remaining family members were seen at their isolated and remote village, and were clinically evaluated at home. They all presented the hearing impairment and communicated with sign language. The facial, auricular, and dental features described above were also present in all the affected members (21 individuals in total; Figure 1) with some intrafamilial variability in the severity of these features (Figure 2a–n). Ear abnormalities were present with

asymmetrical involvement and more prominent dysplastic changes in the upper half of the ear and helix. No family member who is unaffected shared any of the unusual clinical features observed in the affected individuals.

Linkage analysis and fine mapping

This six-generation family contained 21 individuals with hearing loss whose age ranged from 1 to 50 years. Genotyping of 40 consented individuals including affected subjects, parents and siblings was performed using a genome wide 10K SNP array (average resolution of ~0.3 cM) from Affymetrix. Multipoint parametric linkage analysis resulted in a maximum lod score of 10.14 at rs1938684 within an interval defined by rs1404501 and rs2912 (14.6 Mb) (Figure 4). High-density mapping surrounding the linked locus was performed with five additional fluorescently labeled microsatellite markers (D11S913, D11S987, D11S4113, D11S4136, and D11S4162). Recombination events in individuals IV:11 and IV:2 (Figure 1) established the proximal and distal boundaries at D11S4113 and D11S4162, respectively defining a critical region of 2.13 Mb containing 17 annotated genes (Figure 4). Haplotypes of the critical region in affected individuals were consistent with a single founder mutation as may be expected for a rare recessive disease in an extended family.

Candidate gene selection and sequencing

Centrally located within the critical region were three fibroblast growth factors, *FGF19*, *FGF4*, and *FGF3* (Figure 4).

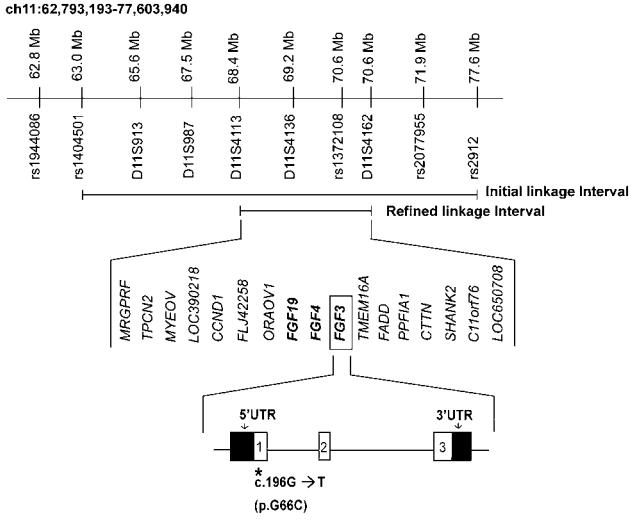

Figure 4 Genotyping of the 11q12.3–14.1 locus for the family is shown. Polymorphic rs1404501 and rs2912 SNP markers defined the initial linkage interval (14.6 Mb). Microsatellite markers D11S913 and D11S4162 defined the refined critical region (2.13 Mb), which contains 17 genes. Among these are three FGF genes *FGF19*, *FGF4*, and *FGF3*. *FGF3*, the gene containing the novel mutation for this family with its 3 exons is shown.

FGF19 plays an important role in several physiological functions, including angiogenesis, mitogenesis, pattern formation, cellular differentiation, metabolic regulation, tissue repair, and oncogenesis.[21] Ladher *et al*[22] presented evidence for mesodermal initiation of otic development in chick embryos and showed that the synergistic interactions of the extracellular polypeptide ligands, fgf19 and wnt8c initiate the inner ear development. Represa *et al*[23] showed that *fgf3* constitutes a signal for induction of the otic vesicle, the primordium of the inner ear; *fgf3* transcripts were detected in the rhombencephalon of a mouse embryo at a developmental stage when the induction of the inner ear occurs. Recently, Hatch *et al*[24] showed, in a mouse, that *fgf3* which is expressed in the hindbrain and in the prospective neurosensory domain of the otic epithelium during morphogenesis initiation, is required for both auditory and vestibular function. Although *FGF4,* unlike *FGF19* and *FGF*3, is not known to have a developmental role that can explain the phenotype of the family being studied, it was screened based on its physical localization between *FGF19* and *FGF3*. The entire coding region of *FGF19*, *FGF4* and *FGF3* was screened for the presence of mutations by direct sequencing. In doing so, we identified a novel homoallelic missense mutation (c.196G→T) in the first exon of *FGF3* (Figure 5) in all 21 affected individuals who participated in this study. All parents of affected individuals were as expected heterozygous carriers and unaffected siblings and relatives were also either carriers or homoallelic for the wild-type G allele (Figure 5). This mutation substitutes the simplest amino acid glycine with cysteine (p.G66C), a sulfhydryl-forming amino acid. The glycine residue is highly conserved across a broad range of species.[25] Novelty of the c.196G→T variation was confirmed by its absence in more than 200 chromosomes derived from the normal Saudi population.

Discussion

Positional cloning using a large consanguineous Saudi family with syndromic deafness was carried out, and identified a novel missense mutation of *FGF3*. This report provides an independent confirmation of the causal link between *FGF3* and a syndromic form of hearing loss similar to that reported recently.[13] Despite the established role of *fgf3* in murine inner ear development,[24] these reports represent the first examples of a human birth defect caused by *FGF3* mutations and is and yet another example of an oncogene, mutations of which can have teratogenic consequences (other examples include c-kit and *GLI3*).

The phenotype of the Saudi family reported in this study is consistent with those reported by Tekin *et al*.[13] In common with the three Turkish families reported, affected members in this study were of normal weight, height and

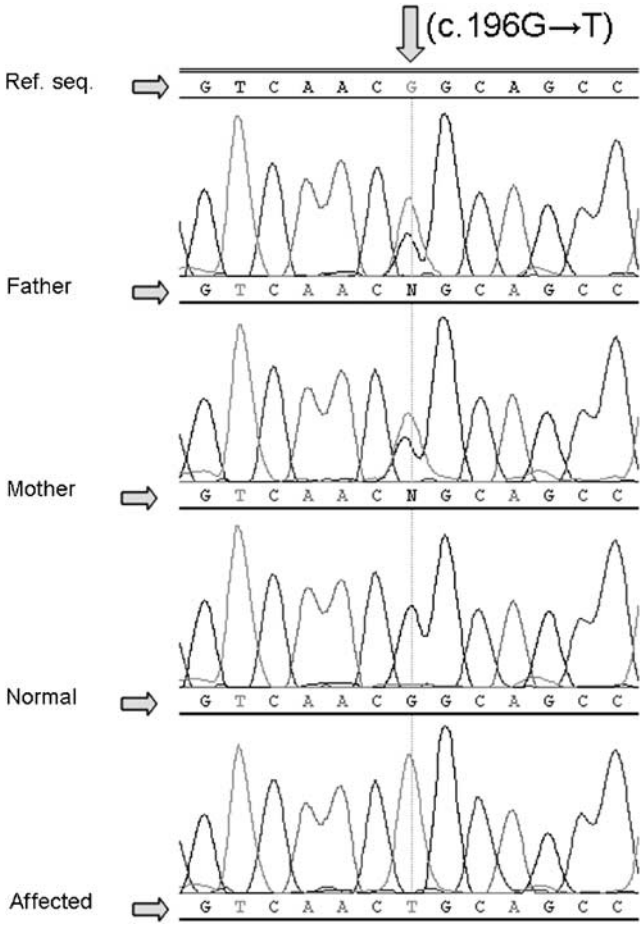

Figure 5 Sequence electrograms of wild-type (reference sequence), heterozygous carrier parents, and one homozygous-affected individual having the novel nonsense c.196G→T mutation is shown.

head circumference. The three major phenotypic features, profound congenital sensorineural deafness, microdontia with widely spaced teeth and type 1 microtia with shortened auricles above the crura of antihelix were in common with all Turkish families and the Saudi family from this study. A complete absence of the inner ear structures on the right side and a rudimentary cystic vestibular structure on the left side (Michel aplasia),[26] with essentially normal external and middle ear structures was also evident and in common with this and the Turkish study. Our results further support the identification of this syndromic form of congenital sensorineural deafness resulting from mutation of *FGF3*.

In this study, we describe a novel missense mutation resulting in the substitution of glycine with cysteine at residue 66 of FGF3. Although this residue is outside of domains either promoting or inhibiting nuclear localization,[27] the introduction of cysteine at residue 66 in addition to native cysteine residues at position 50 and 115 of FGF3 may result in the alteration of a secondary structure that results in loss of function or affects nuclear localization. However, amino acid sequence alignment of 18 FGF family members (homology of 15–55%) using three different alignment algorithms led essentially to an identical set of conserved amino acids.[25] No pattern was evident from location of these amino acids in the primary sequence or in the number of intervening residues. Despite limited sequence identity between FGF prototype members FGF1 and FGF2, C^{α} traces of these proteins superimpose in several independent crystal structures and is consistent with all FGF family members having in common a 'β-trefoil fold'.[28–30] Of 26 amino acids conserved in FGF family members 7 are glycine/proline and 13 are hydrophobic. Mapping of these onto the three-dimensional structure of FGF2 indicated that the glycine/proline almost always form turns between the β-sheets. These glycine/proline are apparently part of the structural scaffold of FGF.[25] In this study, the G66C mutation of FGF3 involves a glycine residue conserved in 18 FGF family proteins,[25] and is likely to disrupt the 'β-trefoil fold' a consequence of which may be a loss of function or impairment of nuclear localization and therefore, resultant pathogenicity.

Thus far, no studies have been done to investigate the functional effect of mutations in *FGF3*. It is tempting to speculate a loss of function model as the mutation spectrum reported by Tekin *et al*,[13] only included a frameshift mutation and a truncating mutation. However, both of the latter two mutations are expected to preserve at least the first 104 N-terminal amino acids (assuming that the truncating mutation does not elicit nonsense-mediated RNA decay), a region that includes the two signal motifs that compete to determine the nucleus/nucleolus *vs* secretory fate of the protein,[31] thus possibly operating as hypomorphic mutations in the heterozygous state. This is further supported by the recent finding that *FGF3* hemizygosity underlies oto-dental syndrome,[32] a disorder with a great degree of overlap with the phenotype described by Tekin *et al*[13] and this paper. As carriers in our family and those described by Tekin *et al*[13] were phenotypically normal, it seems unlikely that their mutations were amorphic in nature. Functional analysis will be needed to better understand the molecular and pathogenic mechanisms of these mutations.

References

1 Morton NE: Genetic epidemiology of hearing impairment. *Ann NY Acad Sci* 1991; **630**: 16–31.
2 Petit C: From deafness genes to hearing mechanisms: harmony and counterpoint. *Trends Mol Med* 2006; **12**: 57–64.
3 Morton CC, Nance WE: Newborn hearing screening – a silent revolution. *N Engl J Med* 2006; **354**: 2151–2164.
4 Smith RJ, Bale Jr JF, White KR: Sensorineural hearing loss in children. *Lancet* 2005; **365**: 879–890.
5 Alvarez Y, Alonso MT, Vendrell V *et al*: Requirements for FGF3 and FGF10 during inner ear formation. *Development* 2003; **130**: 6329–6338.

6 Ladher RK, Wright TJ, Moon AM *et al*: FGF8 initiates inner ear induction in chick and mouse. *Genes Dev* 2005; **19**: 603–613.
7 Zelarayan LC, Vendrell V, Alvarez Y *et al*: Differential requirements for FGF3, FGF8 and FGF10 during inner ear development. *Dev Biol* 2007; **308**: 379–391.
8 Ohyama T, Mohamed OA, Taketo MM *et al*: Wnt signals mediate a fate decision between otic placode and epidermis. *Development* 2006; **133**: 865–875.
9 Chang W, Brigande JV, Fekete DM *et al*: The development of semicircular canals in the inner ear: role of FGFs in sensory cristae. *Development* 2004; **131**: 4201–4211.
10 Pirvola U, Spencer-Dene B, Xing-Qun L *et al*: FGF/FGFR-2(IIIb) signaling is essential for inner ear morphogenesis. *J Neurosci* 2000; **20**: 6125–6134.
11 Ohuchi H, Yasue A, Ono K *et al*: Identification of cis-element regulating expression of the mouse Fgf10 gene during inner ear development. *Dev Dyn* 2005; **233**: 177–187.
12 Pauley S, Wright TJ, Pirvola U *et al*: Expression and function of FGF10 in mammalian inner ear development. *Dev Dyn* 2003; **227**: 203–215.
13 Tekin M, Hismi BO, Fitoz S *et al*: Homozygous mutations in fibroblast growth factor 3 are associated with a new form of syndromic deafness characterized by inner ear agenesis, microtia, and microdontia. *Am J Hum Genet* 2007; **80**: 338–344.
14 Miller SA, Dykes DD, Polesky HF: A simple salting out procedure for extracting DNA from human nucleated cells. *Nucleic Acids Res* 1988; **16**: 1215.
15 Dean FB, Hosono S, Fang L *et al*: Comprehensive human genome amplification using multiple displacement amplification. *Proc Natl Acad Sci USA* 2002; **99**: 5261–5266.
16 Matsuzaki H, Loi H, Dong S *et al*: Parallel genotyping of over 10 000 SNPs using a one-primer assay on a high-density oligonucleotide array. *Genome Res* 2004; **14**: 414–425.
17 O'Connell JR, Weeks DE: PedCheck: a program for identification of genotype incompatibilities in linkage analysis. *Am J Hum Genet* 1998; **63**: 259–266.
18 Abecasis GR, Cherny SS, Cookson WO *et al*: Merlin – rapid analysis of dense genetic maps using sparse gene flow trees. *Nat Genet* 2002; **30**: 97–101.
19 Gudbjartsson DF, Jonasson K, Frigge ML *et al*: Allegro, a new computer program for multipoint linkage analysis. *Nat Genet* 2000; **25**: 12–13.
20 Kambouris M, Banjar H, Moggari I *et al*: Identification of novel mutations in Arabs with cystic fibrosis and their impact on the cystic fibrosis transmembrane regulator mutation detection rate in Arab populations. *Eur J Pediatr* 2000; **159**: 303–309.
21 Nishimura T, Utsunomiya Y, Hoshikawa M *et al*: Structure and expression of a novel human FGF, FGF-19, expressed in the fetal brain. *Biochim Biophys Acta* 1999; **1444**: 148–151.
22 Ladher R, Anakwe K, Gurney A *et al*: Identification of synergistic signals initiating inner ear development. *Science* 2000; **290**: 1965–1967.
23 Represa J, Leon Y, Miner C *et al*: The int-2 proto-oncogene is responsible for induction of the inner ear. *Nature* 1991; **353**: 561–563.
24 Hatch EP, Noyes CA, Wang X *et al*: Fgf3 is required for dorsal patterning and morphogenesis of the inner ear epithelium. *Development* 2007; **134**: 3615–3625.
25 Venkataraman G, Raman R, Sasisekharan V *et al*: Molecular characteristics of fibroblast growth factor-fibroblast growth factor receptor-heparin-like glycosaminoglycan complex. *Proc Natl Acad Sci USA* 1999; **96**: 3658–3663.
26 Michel P: Memoire sur les anomalies congenitales de poreille intern. *Gazette Med de Strasburg* 1863; **23**: 55–58.
27 Antoine M, Reimers K, Dickson C *et al*: Fibroblast growth factor 3, a protein with dual subcellular localization, is targeted to the nucleus and nucleolus by the concerted action of two nuclear localization signals and a nucleolar retention signal. *J Biol Chem* 1997; **272**: 29475–29481.
28 Eriksson AE, Cousens LS, Matthews BW: Refinement of the structure of human basic fibroblast growth factor at 1.6 A resolution and analysis of presumed heparin binding sites by selenate substitution. *Protein Sci* 1993; **2**: 1274–1284.
29 Zhang JD, Cousens LS, Barr PJ *et al*: Three-dimensional structure of human basic fibroblast growth factor, a structural homolog of interleukin 1 beta. *Proc Natl Acad Sci USA* 1991; **88**: 3446–3450.
30 Zhu X, Komiya H, Chirino A *et al*: Three-dimensional structures of acidic and basic fibroblast growth factors. *Science* 1991; **251**: 90–93.
31 Antoine M, Reimers K, Wirz W *et al*: Fibroblast growth factor 3, a protein with a dual subcellular fate, is interacting with human ribosomal protein S2. *Biochem Biophys Res Commun* 2005; **338**: 1248–1255.
32 Gregory-Evans CY, Moosajee M, Hodges MD *et al*: SNP genome scanning localizes oto-dental syndrome to chromosome 11q13 and microdeletions at this locus implicate FGF3 in dental and inner-ear disease and FADD in ocular coloboma. *Hum Mol Genet* 2007; **16**: 3482–3493.